Materials and Structures (2024) 57:82
https://doi.org/10.1617/s11527-024-02347-5

ORIGINAL ARTICLE

Bond of textile-reinforced belite calcium sulfoaluminate cement mortar to concrete substrate

Szymon Cholostiakow · Zhili Ren · Ioanna Skyrianou · Lampros Koutas · Christos Papakonstantinou · Eric Bescher · Theodore Hanein

Received: 12 December 2023 / Accepted: 29 March 2024

Abstract The fast aging of existing building stock requires effective and sustainable strengthening solutions. Textile-reinforced mortars (TRM) have already proved to be very effective as well as versatile retrofitting solutions for reinforced concrete and masonry structures. TRMs can enhance the load bearing capacity of reinforced concrete structures; however, current TRM systems are based on standard Portland cement-based binders, which largely contribute to global human-induced CO_2 emissions. This work, for the first time, explores the use of belite calcium sulfoaluminate (BCSA) binder for carbon textile reinforcement through a cross-disciplinary study combining structural engineering and materials science. An experimental study was carried out on concrete block members with externally bonded strips of carbon textile-reinforced mortars, similar to a typical TRM retrofitting system for concrete beams. The textiles were embedded in an ordinary Portland cement-based (OPC) binder or in a BCSA-based binder to compare the bond behaviour to the concrete substrate. The tests revealed a superior bond between the BCSA mortar and the concrete, as well as outstanding adhesion to the textiles achieved using the BCSA binder, with performance levels largely surpassing those measured in their counterparts that used the OPC-based binder. Scanning Electron Microscopy, X-ray diffraction, and thermogravimetric analyses were used to understand this behaviour difference and it was concluded that the ettringite phase is responsible for the enhanced performance in the studied system. The results of this study suggest that BCSA binders have the potential to be a more effective and

Supplementary Information The online version contains supplementary material available at https://doi.org/10.1617/s11527-024-02347-5.

S. Cholostiakow (✉) · I. Skyrianou · L. Koutas · C. Papakonstantinou
Department of Civil Engineering, University of Thessaly, Volos, Greece
e-mail: simon.cholost@gmail.com

I. Skyrianou
e-mail: iskyrianou@uth.gr

L. Koutas
e-mail: koutas@uth.gr

C. Papakonstantinou
e-mail: cpapak@uth.gr

Z. Ren · T. Hanein (✉)
Department of Materials Science and Engineering, University of Sheffield, Sheffield, UK
e-mail: theodorehanein@gmail.com

Z. Ren
e-mail: zren18@sheffield.ac.uk

E. Bescher
Department of Materials Science and Engineering, University of California, Los Angeles, USA
e-mail: bescher@ucla.edu

T. Hanein
Manatee Consulting Limited, Sheffield S3 7XL, UK

Published online: 30 April 2024

"greener" alternative to the standard binders based on Portland cement in TRM strengthening applications.

Keywords Bond · Belite calcium sulfoaluminate cement · BCSA · Reinforced concrete · Textile-reinforced mortar · Ettringite

1 Introduction

The ageing of reinforced concrete (RC) is a natural process and while this material is known for its long lifespan, it is still susceptible to certain forms of deterioration due to corrosion of the steel reinforcement, fatigue, overload, lack of maintenance, and severe environmental exposure. A large portion of the existing RC building stock was constructed back in the '60 s and '70 s and is now approaching its designed life span. Some structures have already surpassed their designed life and the safety of their structural elements is now compromised, thus warranting immediate rehabilitation or strengthening. Most RC structures, especially those built using outdated design provisions, were designed for a service life of approximately 50 years; therefore, an ever-increasing number of structures will need major maintenance or strengthening. Recent surveys report that 42% of 617,084 highway RC bridges in the USA are already over 50 years old and 12% are already 80 years old [1]. According to the European Construction Industry Federation [2], the renovation of existing buildings comprised more than 27% of the main construction activities in Europe in 2021, amounting to over 313 billion euros with 5.7% annual growth rate, which clearly highlights the scale of this arising problem.

In recent years, the safety of old RC buildings has significantly improved owing to novel structural retrofitting systems utilising advanced composite materials which are resistant to corrosion, are lightweight, and can significantly prolong structures' lifespan. The first generation of such composites, which gained their popularity in the late '90 s, are the Fibre-Reinforced Polymers (FRP) [3], comprising laminates made of high-strength continuous fibres (e.g. carbon, glass, aramid) embedded in a polymeric matrix (typically epoxy resin), which can be externally bonded to the surface of structural elements to enhance their load bearing capacity [4–7], and thus improve the safety and longevity of the whole structure. However, several drawbacks related to the use of epoxies in FRP systems (e.g. incompatibility with masonry substrates, poor performance at elevated temperatures and UV exposure) required seeking alternative solutions for specific applications [8]. In the mid '00 s, the second generation of advanced composites was introduced [9–11]; namely the Textile-Reinforced Mortars (TRM), which replaced organic matrices (epoxies) with inorganic mortars (typically cement-based), hence addressing the limitations of the epoxy-based systems. TRM systems use fibres in an open-mesh configuration (textiles) instead of continuous fibre rovings embedded in resin as in the case of FRP systems. TRMs have been successfully used in a wide range of applications [12–14] as well as to retrofit existing structures [15], and have proven to be versatile and an effective strengthening solution for both RC [8] and masonry structures [16].

The strengthening performance of TRM systems relies mostly on the bond strength of the mortar-textile interfaces, which in many cases determines the failure behaviour. Organic matrices like epoxy-based resins develop better bond with the fabrics, however, in inorganic-based systems this bond can be limited. In epoxy-based matrices the fibres are fully impregnated with resin and the main bond mechanism occurs through chemical bonding. Conversely, in inorganic-based matrices, where voids are present at the textile-matrix interface, the bond mechanisms involve a combination of chemical bond and mechanical interlock. An enhanced bond between the materials improves the composite action, thus allowing for a better utilisation of the retrofitting and, in turn, a higher strengthening efficiency [17]. The mortar-textile bond efficiency depends on the level of the textiles' impregnation with the mortar's paste, and thus on the quantity of fibres that are effectively engaged in resisting load. Most studies dealing with bond in TRM systems have mainly focused on the use of different types of textiles and substrates [18–26] and have greatly contributed to the current state-of-the-art. However, the lack of research on the effect of the matrices of TRM systems might carry the notion that the type of textile and the substrate have the main influence on the strengthening performance. In contrast, the recent findings of the authors showed that the mortar type can also have a significant influence on the effectiveness of the TRM application [27–29].

The choice of the binding matrix does not only have a structural importance; given the large fraction of existing building stock that requires maintenance, it can also have a significant impact on the environment and human life on Earth. The global efforts to reduce human-induced carbon emissions require the use of sustainable low-carbon materials, which can also promote material circularity. The use of binders based on Ordinary Portland Cement (OPC) largely contribute to greenhouse gas emissions [30] and the cement community is actively seeking eco-efficient alternatives, of which several are being developed [31]. One such alternative is belitic calcium sulfoaluminate cement (BCSA), which is a standalone cement that can achieve ~30% less carbon dioxide emissions [32]. This saving can be further increased if alternative sources of alumina (instead of bauxite) are used in the manufacture, such as alumina rich clays and industrial side streams. BCSA cement is known for its early-strength and rapid-setting capabilities brought about mainly through the formation of significant quantities of ettringite [31] (its compressive strength can reach 40 MPa in a few hours) and has been successfully used for the rapid rehabilitation of concrete infrastructure such as runway or highway pavements that require a return to service within a few hours of closure [33, 34]. Although commercialised in the USA since the '70 s, BCSA is not usually familiar to the construction workforce and its efficient use generally requires know-how, for example, due to the fast-setting times which will need expertise for control. While the binder has been used as part of several concrete rehabilitation strategies [35], its use in combination with advanced composite systems has never been studied.

This study, for the first time, investigates the bond behaviour of carbon textile-reinforced BCSA mortar (BCSA TRM) to concrete substrate. The bond is experimentally assessed by means of modified beam hinge test for different bond lengths. The tests are compared with tests on specimens having identical carbon textiles embedded in an OPC matrix. The results of the bond tests are complemented with microstructure characterisation through Scanning Electron Microscopy (SEM), X-ray diffraction (XRD), and Thermogravimetric Analyses (TGA) to understand the bond between the binder and the textile. As such, this study offers a fair comparison between TRM systems with different binder chemistries and contributes towards the development of a novel, resilient and sustainable product for rapid structural retrofitting of deteriorated or substandard RC structures.

2 Testing programme

We examined the bond of two carbon textile-reinforced mortar systems to concrete substrate utilising different binders: (i) a standard commercially used mortar mix based on OPC; and ii) a BCSA mortar. The aim of this study was to determine experimentally if the BCSA binder is capable of developing a bond performance matching this of a standard cement-based system, and thus determining if BCSA can be successfully used as a matrix for TRM systems. The BCSA mortar was designed to have similar critical mechanical and physical properties to the OPC binder, hence enabling a fair comparison of the bond behaviour of the two binding agents. The workability and the flexural strength were controlled by adjusting the water and citric acid ratios until comparable values of the OPC binder were achieved on the 35th day of curing. The structural tests comprised nine twin specimens (eighteen in total). The first eight specimens investigated the bond of a standard OPC TRM system, and the next eight specimens served as their counterparts having BCSA mortar. Four bond lengths (50, 100, 150, and 200 mm) were examined to estimate the effective bond length of the two systems, and each test was repeated twice to increase confidence in the results. The last two specimens had BCSA binder, a bond length of 200 mm and were tested after only one day (24 h) of curing following the application to explore the potential of the rapid set properties of the BCSA cement. The structural tests were supported by XRD, TGA, and a detailed SEM and elemental analysis to provide additional insight into the chemical bond between the mortar and the textiles as well as to observe the fibres' impregnation level.

2.1 Test specimens

Geometry details and the properties of the test members are shown in Fig. 1. Each specimen comprised two 120×200×385 mm concrete blocks joined

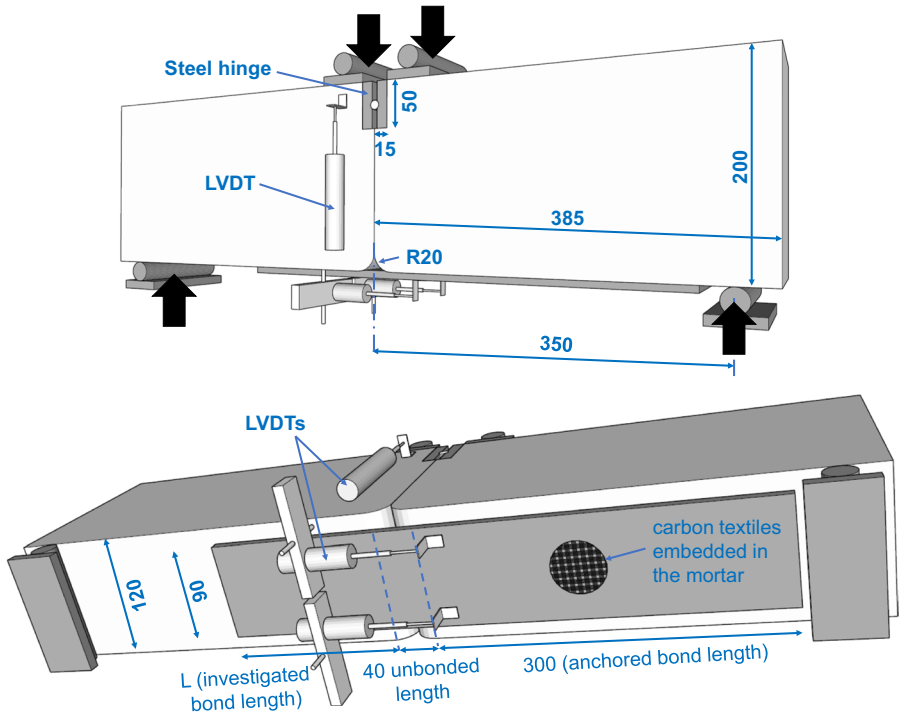

Fig. 1 Dimensions (in mm) and layout of the test specimens; side and bottom view

together by a composite strip bonded in the tensile zone (bottom of the block) and a steel hinge in the compression zone (top of the block). A normal weight concrete was used to cast the blocks, each of them was reinforced with two 8 mm steel rebars at the bottom of the section. At the top of each block an indentation was provided during casting to create space for the steel hinge. The blocks' corners were rounded to a radius of 20 mm to prevent stress concentration in the TRM composite during testing. The mean compressive strength of the hardened concrete was determined by three 150 mm cube specimens at 28 days of curing and was equal to 20.6 MPa with standard deviation equal to 0.52 MPa.

The textile reinforced composite comprised three 90 mm wide plies of high-strength carbon open-mesh textiles embedded in the binding mortar. The bond length on the non-test side was always the same and equal to 300 mm. The bond length on the test side varied from 50 to 200 mm at the intervals of 50 mm. The area in the vicinity of the joint (about 40 mm) was kept unbonded to help accommodate the curvature of the strip during testing. All TRM systems consisted of three carbon textile layers. The names of the specimens were designed to ease the identification of the investigated parameters. For example, OPC_3C_50-1 refers to the first (out of two) specimen with the OPC based binder, three carbon textile layers (3C) and 50 mm bond length (for the full specimen list refer to Table 2). As previously mentioned, four twin specimens (eight in total) investigated the bond of the OPC-based system and corresponding four twin specimens (another set of eight) investigated the bond of the BCSA-based system. Additionally, twin specimens BCSA(24 h)_3C_200_1&2 were tested after just 24 h of curing to determine if the rapid-setting properties of BCSA binder can allow for developing comparable bond behaviour to the OPC-based binder but in much shorter time, which may be critical for some strengthening applications.

2.2 Methodology

2.2.1 Indirect bond tests

The bond was examined through indirect testing employing a modified hinge beam test setup (Fig. 2). In such a setup the tensile force is applied indirectly to the composite strip via a steel hinge located in the compression zone of the beam. This testing method can reproduce the stress state in the TRM composite more realistically compared to direct pull-out tests

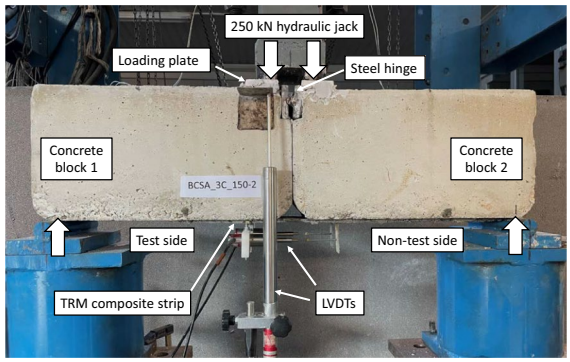

Fig. 2 Modified beam test setup

[36]. The modified beam with the TRM strip bonded to its bottom was simply supported over a 700 mm clear span. After placing the beam in the testing rig, the hinge and the loading plates were bed on a thick gypsum paste ensuring that (i) full contact between the steel parts and the concrete will be achieved and (ii) the TRM strip will be enabled in transferring forces from the onset of testing.

The load was applied under the constant displacement rate of 0.02 mm/s of a 250 kN servo-hydraulic actuator and measured by a load cell connected to the data acquisition system (Fig. 2). The vertical displacement of the concrete blocks was measured using an external Linear Variable Differential Transformer (LVDT) placed under one of the loading points. Two additional LVDTs were placed under the beam to measure the relative displacement of the TRM strip to the concrete block.

2.2.2 Microstructure characterisation

Several samples of the TRM strip were randomly extracted from the concrete block and were subjected to detailed chemical analysis and investigation through scanning electron microscopy (SEM), thus providing further insights into the bond characteristics at material level. The chemistry of BCSA hydration products differs significantly from OPC hydration products, hence it was necessary to identify the phases/minerals present in the samples and assess the degree of hydration. For this reason, X-ray diffraction (XRD) and thermogravimetric analyses (TGA) were also carried out. SEM and energy dispersive X-ray spectroscopy (EDS) were conducted to visualise the bond between the textile fibres and the binder at the micro level as well as identify the chemistry of the binder surrounding the fibres. The details of the XRD analysis are included in the Supplementary Materials.

For the purpose of the SEM analyses, the samples were cut to get fresh sections and following that the samples were embedded in a low-viscosity epoxy resin under a vacuum to impregnate resin into the pores and the gap between mortar and fibres. After the resin hardened, the sections were ground and polished using SiC paper in the order of P400, P800 and P1200 grades, and subsequently were polished with oil-based diamond suspensions of particle size of 15, 6, 3, 1 and 0.25 µm. Before SEM testing, the polished sections were coated with 10 nm carbon. The images were collected in backscattered electrons (BSE) mode and characteristic X-rays (EDS) from SEM instrument (Inspect F50, FEI, America) with a voltage of 10 kV and 20 kV, respectively. The EDS map data was analysed using edxia [37].

2.3 Materials

2.3.1 Binding mortar

A standard commercially used ordinary Portland cement-based (OPC) mortar was selected as a benchmark for further comparisons with the designed BCSA mortar. The mortar dry mix comprised cement, aggregates with maximum size of 1.0 mm and polypropylene microfibres. The desired workability was achieved by mixing water at a fixed water-to-dry-mix ratio of 0.25 (by weight). The consistency of the fresh mortar was determined experimentally according to EN 1015-3 [38] and served as a target consistency for the BCSA mortar. The recorded flow values were equal to 191 mm and 194 mm measured at right angles to one another. The tests on hardened mortar samples carried out according to EN 1015-11 [39] after 35 days of curing, revealed mean flexural strength equal to 7.58 MPa with a standard deviation of 0.71 MPa. The mean compressive strength determined on standard 40 mm cubes was 30.84 MPa with a standard deviation of 2.0 MPa.

A custom BCSA mortar mix was designed for the purpose of this study. To perform a fair comparison of the performance of the two binding mortars, the authors aimed to develop the BCSA binder having fresh and hardened mix properties similar to the

cement-based reference mortar. Flexural strength (modulus of rupture) was particularly important as it represents a measure of the tensile strength in elements subjected to bending. As such, the maximum aggregate size was kept below 1 mm and the ratio between water and cementitious materials was set to 0.185. In addition, 6 mm polypropylene fibres were added in amount of 0.1% by volume to replicate the counterpart OPC mix and make the comparison of the two binders as fair as possible. The workability of the fresh mortar mix was controlled using 1.5% solution of citric acid, which can serve as a retarder. This allowed achieving similar consistency and working time (about 30 min) of the mortar mix based on the OPC. The flow values for the fresh BCSA mortar were 197 and 198 mm, hence in similar range to its OPC-based counterpart. Owing to the rapid strength increase in BCSA, the properties of the hardened mix could be determined within the first few hours of setting. Therefore, to gain insight into the pace of the strength development, the mechanical properties were tested after 1 day, 7 days, and, as in the case of the OPC binder, after 35 days (Fig. 3). As can be seen, a slightly higher value of the 35 day flexural strength was attained compared to the OPC binder. However, given the considerable deviation in the results usually present in brittle materials, some scatter between the two binders was expected, and the two binders were still deemed to be fair materials to compare. Due to the different chemistry, the BCSA binder had much higher compressive strength; yet this should not pose any significant influence on the bond behaviour, as this is mostly governed by the tensile properties of the mortar, which flexural strength can well represent.

2.3.2 *Textile reinforcement*

Three layers of high-strength carbon textiles were used for the TRM composite. A commercially available non-coated carbon textile was employed having a mesh size of 10 × 10 mm and a total weight equal to 170 g/m^2 (see Table 1 and Supplementary Materials). The weight was equally distributed in the two main orthogonal directions of the fibre rovings, thus resulting in 85 g/m^2 per direction and an equivalent thickness of 0.048 mm per direction (given carbon fibres' density of 1.83 g/cm^3).

It is worth noting that the mechanical properties listed in Table 2 refer to the properties of the dry fibres as declared by the manufacturer. The strength of the textile is usually significantly lower than the strength of the dry fibres due to (i) non-uniform stress distribution of all the fibres in a roving, (ii) non-uniform fibre impregnation with the mortar, and iii) decrease of the impregnation level with increasing number of the textile layers [17]. Given that optimal

Table 1 Mechanical properties of the carbon textile used in this study (as given by the manufacturer)

Property	Value
Elastic modulus of the fibres, E_f (GPa)	252
Fibre density, ρ_f (g/cm^3)	1.83
Mesh size (mm × mm)	10 × 10
Surface weight (g/m^2)	170
Equivalent thickness per direction, t_f (mm)	0.048
Tensile strength (kN/m)	240
Elongation at failure, ε_f (%)	2.0

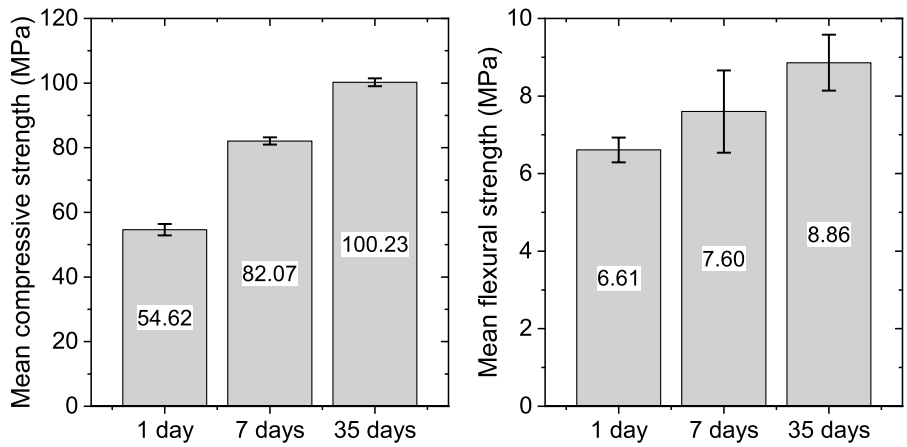

Fig. 3 BCSA mortar strength development over 35 days of curing at room temperature

Table 2 Main results of bond tests

Specimen	P_{max} (kN)	$P_{max,ave}$ (kN)	δ_{max} (mm)	σ_{ave} (MPa)	$\sigma_{ave}/E_f\varepsilon_f$ (%)	Failure mode[1]
OPC_3C_50_1	6.73	6.41	0.78	439.6	8.8	INT
OPC_3C_50_2	6.09		0.91			INT
OPC_3C_100_1	7.88	7.76	1.61	531.9	10.6	INT
OPC_3C_100_2	7.63		1.53			INT
OPC_3C_150_1	11.36	11.78	2.28	807.6	16.2	INT + DCC
OPC_3C_150_2	12.19		2.54			INT + DCC
OPC_3C_200_1	7.52	7.45	2.09	511.0	10.2	INT
OPC_3C_200_2	7.38		2.75			INT
BCSA _3C_50_1	14.04	11.74	1.49	805.5	16.1	DCC
BCSA _3C_50_2	9.44		1.06			DCC
BCSA _3C_100_1	20.91	18.80	3.00	1289.4	25.8	FR
BCSA _3C_100_2	16.69		1.67			DCC
BCSA _3C_150_1	17.80	19.68	2.49	1349.5	27.0	DCC
BCSA _3C_150_2	21.55		3.32			DCC
BCSA _3C_200_1	22.17	22.54	2.74	1545.6	30.9	FR
BCSA _3C_200_2	22.90		3.25			FR
BCSA(24 h)_3C_200_1	5.72	5.74	1.74	393.7	7.9	INT
BCSA(24 h)_3C_200_2	5.76		1.34			INT

[1]*INT* interlaminar shear failure, *DCC* debonding at the mortar-concrete interface with the adjacent concrete cover, *FR* fibre rupture

TRM strengthening applications usually comprise of 2–3 TRM layers, three textile layers were chosen to be investigated to serve as a lower bound of the impregnation level and, thus inform about minimum stress utilisation levels in the TRM. With fewer textile layers the impregnation level would be greater and this would lead to higher fibre utilisation.

3 Bond test results

The main test results for all specimens are shown in Table 2. The recorded measurements include: the peak load (P_{max}) and the vertical displacement at peak load (δ_{max}). The computed values for each set of identical specimens included average load capacity calculated as a mean value between the two tests ($P_{max,ave}$), and average normal stress in the TRM composite (σ_{ave}), which is equal to the tensile force in the textile divided by the area of the textile fibres. The ratio $\sigma_{ave}/E_f\varepsilon_f$ represents the level of the fibre utilisation compared to the ultimate tensile capacity of the carbon textile expressed in percentage.

The normal stress in the TRM strip (σ_T) was estimated based on the tensile force in the TRM strip (T), which derived from the force equilibrium of the free-body diagram (Fig. 4). Due to the rotation of the concrete block about the hinge, the lever arm between the compressive force in the hinge and the tensile force in the TRM strip reduces with increasing angle φ [40]. Thus, the tensile force (T) carried by the textiles can be computed as:

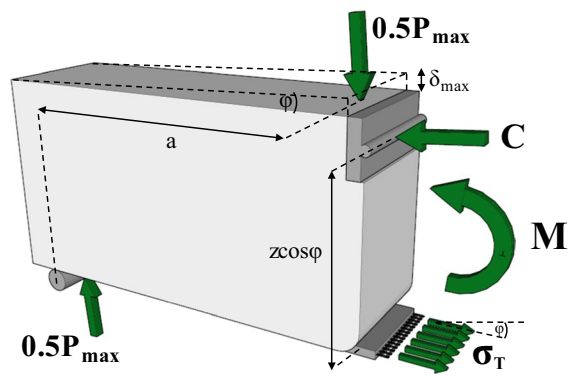

Fig. 4 Free-body diagram for determining tensile stresses in the TRM strip bonded to the concrete block

$$T = \frac{P_{\max}}{2}\frac{\mathrm{a}}{z \bullet \cos\varphi}\cos\varphi = \frac{P_{\max} \bullet \mathrm{a}}{2z} \quad (1)$$

where a is the shear span between the support and the loading point equal to 320 mm and z is the lever arm equal to 180 mm.

The normal stresses (σ_T) in the TRM strip were determined as:

$$\sigma_T = \frac{T}{ntb} \quad (2)$$

where n is the number of textile layers and t and b are the equivalent thickness and width of each textile ply, respectively. The equivalent thickness of one carbon layer was 0.048 mm (Table 1) and the width of the ply was taken as 90 mm (Fig. 1).

3.1 OPC-based composite

All reference tests with OPC-based binder exhibited a common type of cracking behaviour and failure, thus making them a good benchmark for further comparisons with the BCSA binder. Typical failure patterns for the OPC samples are shown in Fig. 5 and Table 2 (see also Supplementary Materials).

The twin samples having bond length from 50 to 150 mm failed on the test side, whereas OPC_200-1 and OPC_200-2 failed on the non-test (longer) side having bond length equal to 300 mm. As mentioned, the predominant failure mode observed in most of the OPC specimens was interlaminar failure (INT) at the textile-binding mortar interface (Table 2, Fig. 5a). The samples OPC_150-1 and OPC_150-2 showed mixed failure patterns involving INT (predominantly) and some minor debonding of the concrete cover (DCC). The limited bond of the mortar to the textiles visible in Fig. 5a may indicate that either the impregnation within the OPC mortar of the three layers of carbon textile was not sufficient to create a strong bond between the materials or the chemical bond to the fibres was limited and governed the failure (or a mix of both). Although both failure mechanisms indicate decent bond to the concrete substrate, the INT failure is associated with poor bond to the textile reinforcement, and hence reduces the efficiency of the strengthening.

The load–deflection curves for all OPC tests are shown in Fig. 6 (red curves). Overall, a good agreement was achieved between the first test and its repetition, which further validates the results and provides additional confidence in the measured values. Despite some minor differences in the initial stiffness, the initial cracking in the TRM developed at fairly similar load levels, around 4 kN. After the onset of cracking, the stiffness reduced but remained similar across the two identical tests until the ultimate load was reached. The highest peak capacity was achieved for the OPC_150 series and was on average equal to 11.75 kN, whereas the lower load capacity was developed by OPC_50_2 and was equal to 6.09 kN.

3.2 BCSA-based composite

The corresponding BCSA series showed significantly improved performance and exhibited superior bonding to the concrete substrate and the textile (Figs. 6 and 7), which allowed to prevent the interlaminar failure mode (INT). Instead, failure occurred

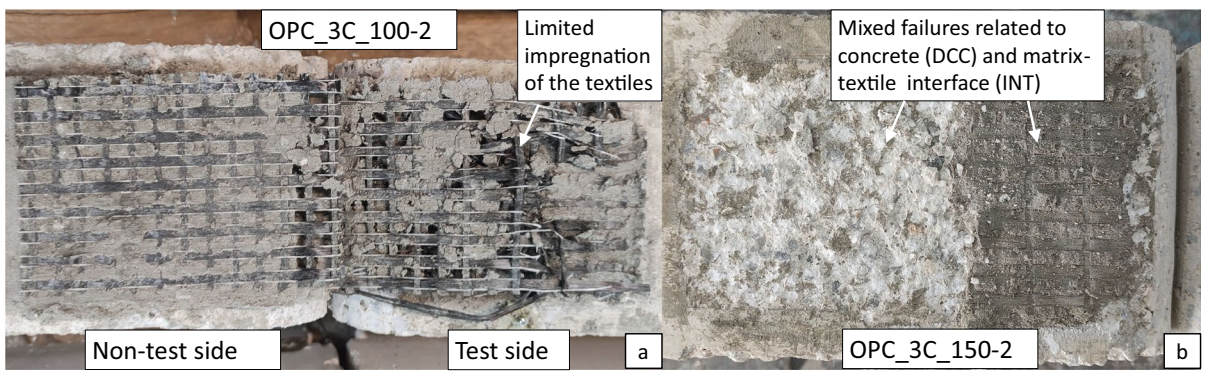

Fig. 5 Typical failure in OPC series: **a** interlaminar failure; **b** interlaminar failure and debonding of concrete cover

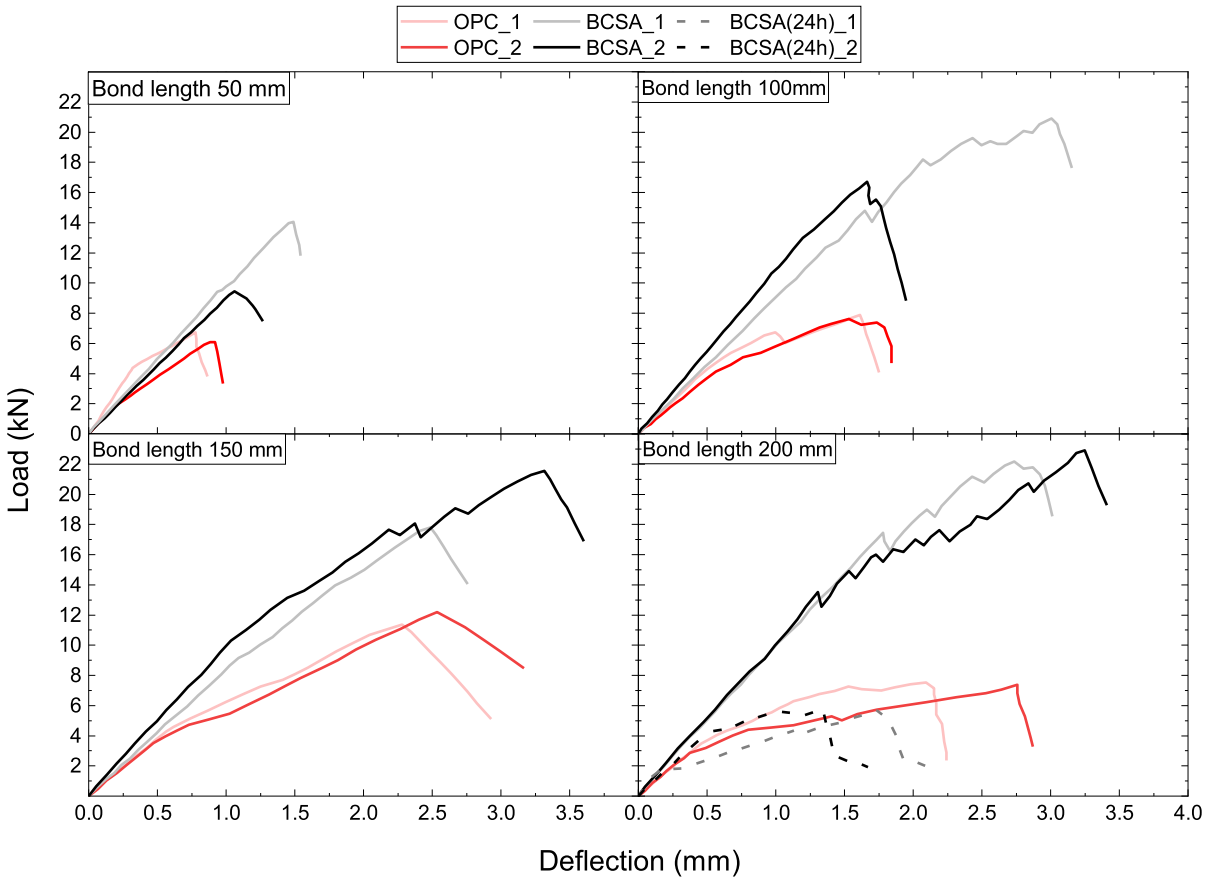

Fig. 6 Load–deflection curves for all specimens

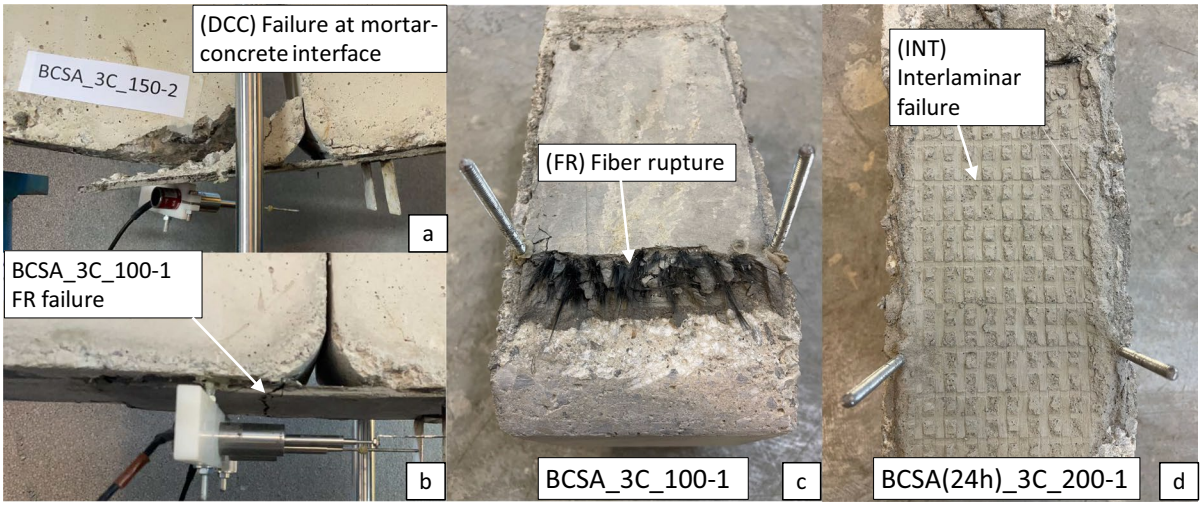

Fig. 7 Typical failure in BCSA series: **a** debonding at the mortar-concrete interface with the adjacent concrete cover (DCC); **b**, **c** fibre rupture (FR); **d** interlaminar failure at textile/mortar interface (INT, only seen in the twin specimens tested after 24 h)

either in the mortar-concrete interface including part of the concrete cover (DCC) or in the textile (FR), thus allowing for a much larger contribution of the carbon fibres to the total load capacity. The failure related to concrete (DCC, Fig. 7) was observed in most of the specimens with bond lengths less than 200 mm, apart from BCSA _3C_100_1 which exhibited rupture of the textile fibres (FR). The former (DCC) was associated with separation of the concrete cover from the RC block at the round corners up to the depth of the steel reinforcement. Such behaviour can be attributed to the fact that in these specimens high bond stresses were distributed over a relatively short distance from the block corner, subjecting it to high stress concentration (similar failures have been already reported before [41]). Specimens BCSA _3C_100_1, BCSA _3C_200_1, and BCSA _3C_200_2 failed predominantly due to the rupture of the textiles with some slippage of the inner fibres within the binder (Fig. 7b, c), which is a common combination of failure mechanisms in TRM applications due to fact that inner fibres have often limited impregnation within the matrix [8]. As such, the carbon textiles in the BCSA systems with larger bond length were exploited to a much higher degree (up to 30%, see Table 2).

Similar load–deflection responses were achieved between the two identical BCSA bond tests (black and grey curves, Fig. 6). The lowest peak capacity (9.44 kN) was achieved by BCSA _3C_50_2, which failed due to sudden detachment of the thin layer of the concrete cover, without any prior signs of cracking in the TRM. Due to the excellent bond, the TRM strip remained firmly attached to the concrete substrate and no cracks were detected in any of the specimens' TRM surface until reaching a load level of about 11 kN (see BCSA _3C_150_2), which was manifested by a slight decrease in the stiffness. The largest capacity was developed in the specimens with the failure related to the textile and reached up to 23 kN for BCSA _3C_200_2. The scatter in the peak loads across two identical tests can be attributed to the different failure patterns and behaviour. The specimens which exhibited failure in the concrete cover recorded fairly lower peak capacity, whereas the failure related to the textile enabled developing larger loads. The difference in the failure behaviour can be partially attributed to the different bond length and bond strength between mortar and fibres. Further discussion is provided in the following sections.

The twin specimens BCSA(24 h)_3C_200_1&2 cured in the same conditions as their counterparts BCSA_3C_200_1&2, but were tested 24 h after the TRM composite application. Both specimens exhibited similar failure mechanism to the specimens with OPC binder tested after 35 days; the failure initiated within the central bottom part of the TRM strip and progressed towards the end of the strip bonded on the 200 mm test side. Similar to the OPC series, the failure occurred between the binder and the first textile layer without any signs of concrete debonding (Fig. 7d), indicating poorer bond behaviour. Even though the bond behaviour of the samples tested after 24 h was visibly poorer, the load–displacement curves are in a close agreement with the OPC samples, with slightly lower peak and displacement capacity attained by the BCSA(24 h) samples (see Table 2). As such, it can be concluded that just after 1 day of curing a BCSA-based TRM system has a potential to develop tensile properties approaching those of the 35 day cured OPC-based TRM system and exhibit similar failure behaviour. For the corresponding mortars the flexural strength values were 6.61 MPa vs. 7.58 MPa for the BCSA(24 h) and OPC, respectively. However, it should be noted that during the first 24 h of curing the strength increase of BCSA is rapid and this could contribute to the variability in the strength. Whilst the two same tests carried out on BCSA(24 h) samples did not show any significant variability, more research is still needed to fully characterise the behaviour of short-time cured TRM composites based on BCSA cements.

4 Microstructure analysis

4.1 BCSA mortar hydration products

4.1.1 X-Ray diffraction analysis

The samples were cut and prepared for the characterisation within 2 weeks after the structural testing and placed in a desiccator with silica gel inside until SEM testing to stop the hydration process. The phases of

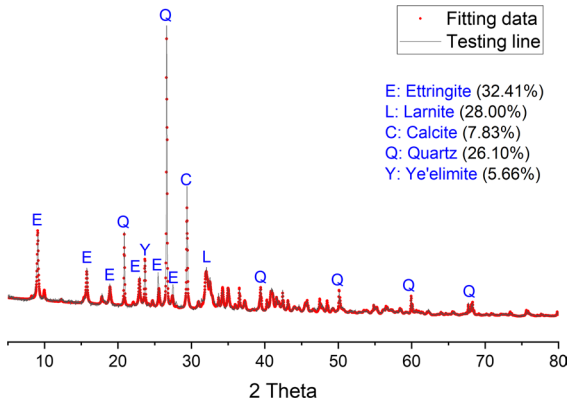

Fig. 8 The XRD curve of BCSA mortar

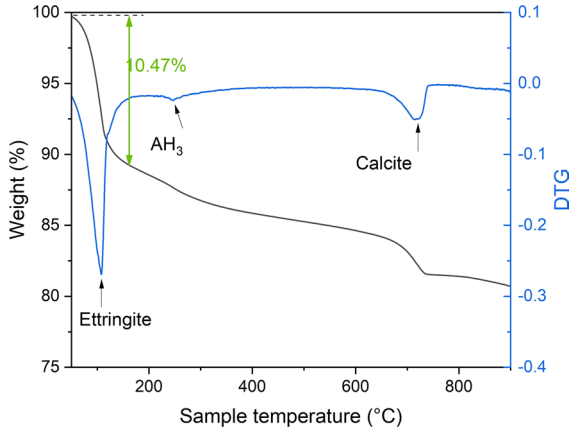

Fig. 9 The TG and DTG data of BCSA composite showing only hydration products of ettringite

BCSA-based composite were studied via X-Ray diffraction analysis (XRD), and Rietveld analysis was conducted using the phases shown in the Supplementary Materials. The fitting curve and relative phase contents are shown in Fig. 8. It should be noted that Rietveld analyses does not account for any amorphous/gel phases such as AH3 or calcium silicate hydrates (C–S–H) formed in the specimen, and the quantity of sand in the specimens leads to an inaccuracy in the amorphous calculation. Hence, the XRD data can only calculate the relative content of crystal phases in BCSA mortar. Figure 8 shows that belite (larnite) was identified because of its low hydraulic reactivity. In addition, a high amount of ettringite, which is the main hydration product of calcium sulfoaluminate cement (CSA), was found in the specimen at age of testing. No stratlingite and calcium aluminate monosulfate (Afm) was detected.

4.1.2 Thermogravimetric analysis

The weight loss was investigated via TG technique, and the result is shown in Fig. 9. The main peak from 30 to 160 °C relates to the dehydration of ettringite [42], the weight loss here is about 10.47%, and some aluminium hydroxide ($Al_2(OH)_3$, AH_3) and calcite formed in the BCSA binders. The weight loss at ~250 °C is attributed to AH_3. Both XRD and TG indicate that ettringite is the major hydration product and that some of the ettringite has carbonated. TG analysis also suggests that no stratlingite water loss is observed.

4.2 Composite microstructure

4.2.1 OPC-based composite

The microstructure of the bond between OPC binder and fibres were observed via back scattered electrons (BSE) images, shown in Fig. 10. The image presents a typical section of the composite at the edge of the carbon fibre bundle and the OPC mortar paste; the approximate interface is shown by the yellow line in Fig. 10a. As can be seen, the level of the fibres' impregnation with the mortar paste is rather limited and the bond to the textiles relies mostly on the fibres located near the interface, thus making the inner fibres (those within the yellow region) not fully engaged during loading. The images show that the space between the fibres is empty and the black regions between the fibres shown in the BSE images are mostly voids filled by the resin used to produce the SEM specimen (Fig. 10b). The resin is present because the sample prior to polishing was embedded in low-viscosity resin in a vacuum to fix the fibres in place. As such, the regions showing resin represent voids and pores in the structure of the composite. This sample BSE image, representing typical interface between the textile and mortar, indicates that the microstructure of the fibre-binder interface is full of voids, and this leads to limited bond and could trigger failure at this interface at relatively low capacity. Such voids

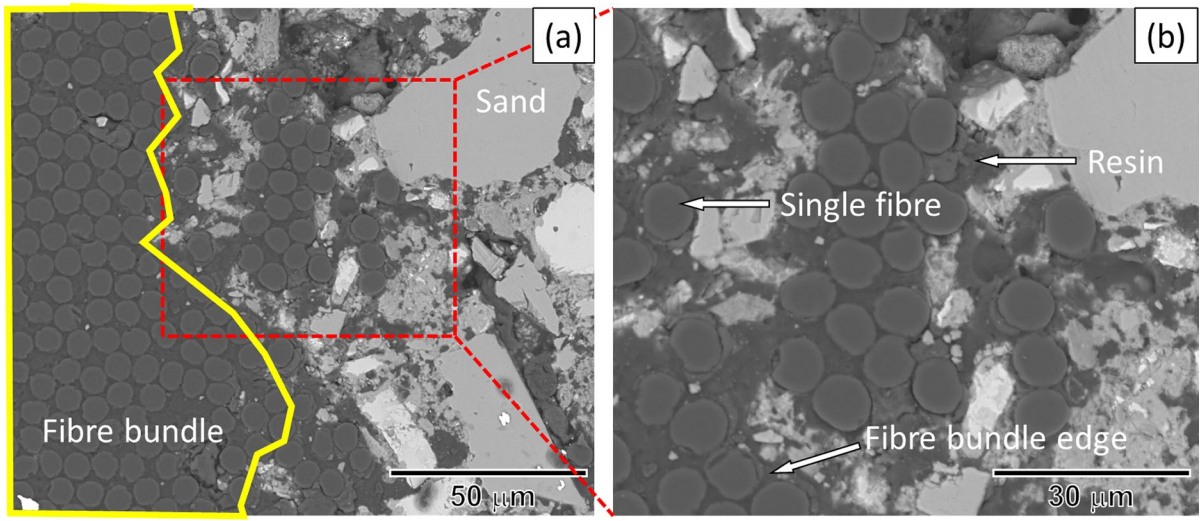

Fig. 10 The BSE images of section of composite made using OPC binder

are seen not only between the single fibres, but also around the fibre bundles, indicating that the bond at the mortar-textile interface is limited (Fig. 10b). This seems to explain well the observed failure mode (INT), which was characterised by interlaminar failure between the plies of the textile at the interface between the textile and the matrix of the OPC composite.

4.2.2 BCSA-based composite

The bond properties of the BCSA-based composite are shown in Fig. 11. Similar to the case of the OPC-based composite, the BCSA binder was unable to penetrate inside the fibre bundle enclosed within the yellow boundary lines shown in Fig. 11a. Compared to the OPC binder, more micro cracks were found in the hardened mortar, but no resin was found in these cracks indicating the cracks

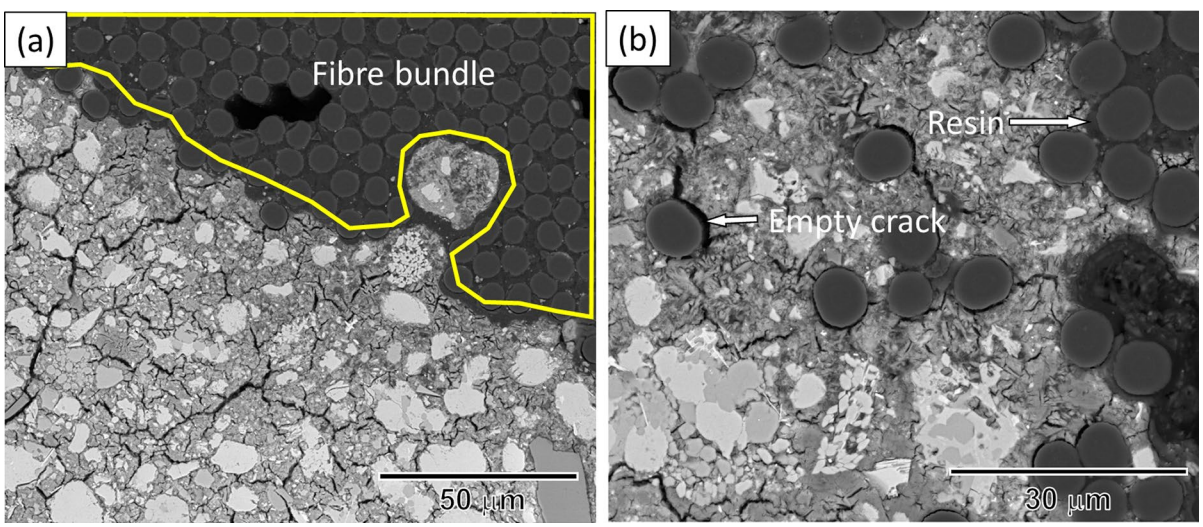

Fig. 11 The BSE images of sections of BCSA

developed after the epoxy impregnation process. The polished sample was placed in a desiccator with silica gel inside for a few weeks before SEM testing to stop the hydration process, which could cause some cracks due to the dry environment. Bizzozero et al. [43] found that the drying process can lead to such cracks in the CSA samples, hence, some of the cracks around the fibres shown in Fig. 11a and b could have been developed upon drying.

Despite the above, the BCSA composite showed enhanced bond performance, which effectively engaged more fibres and shifted the failure from the mortar-textile interface to the mortar-concrete interface and further to the textile itself for larger bond lengths. As can be seen in Fig. 11, fewer voids could be identified at the edge of the fibre bundle and mortar paste was more adjacent to the fibres, thus increasing bonding between the two. It is deemed that the enhanced bond performance in the BCSA-based composite is related to the hydraulic products around the fibres and the ettringite phase which developed at the interface. An EDS map analysis was conducted to analyse the phases and visualise the hydrated products around the fibres (Fig. 12).

Based on the element distributions observed from Fig. 12a, c and d, a high concentration of sulfate (S) and aluminate (Al) was found around the fibres. The S/Ca and Al/Ca ratios are plotted in Fig. 12b to identify chemistry around the fibres for these specific regions. The average values were equal to S/Ca = 0.43 and Al/Ca = 0.36, revealing that these phases are mainly ettringite. This phase is characterised by needle-like products and such ones have been identified between the fibres at the edge of the bundle (Fig. 13)

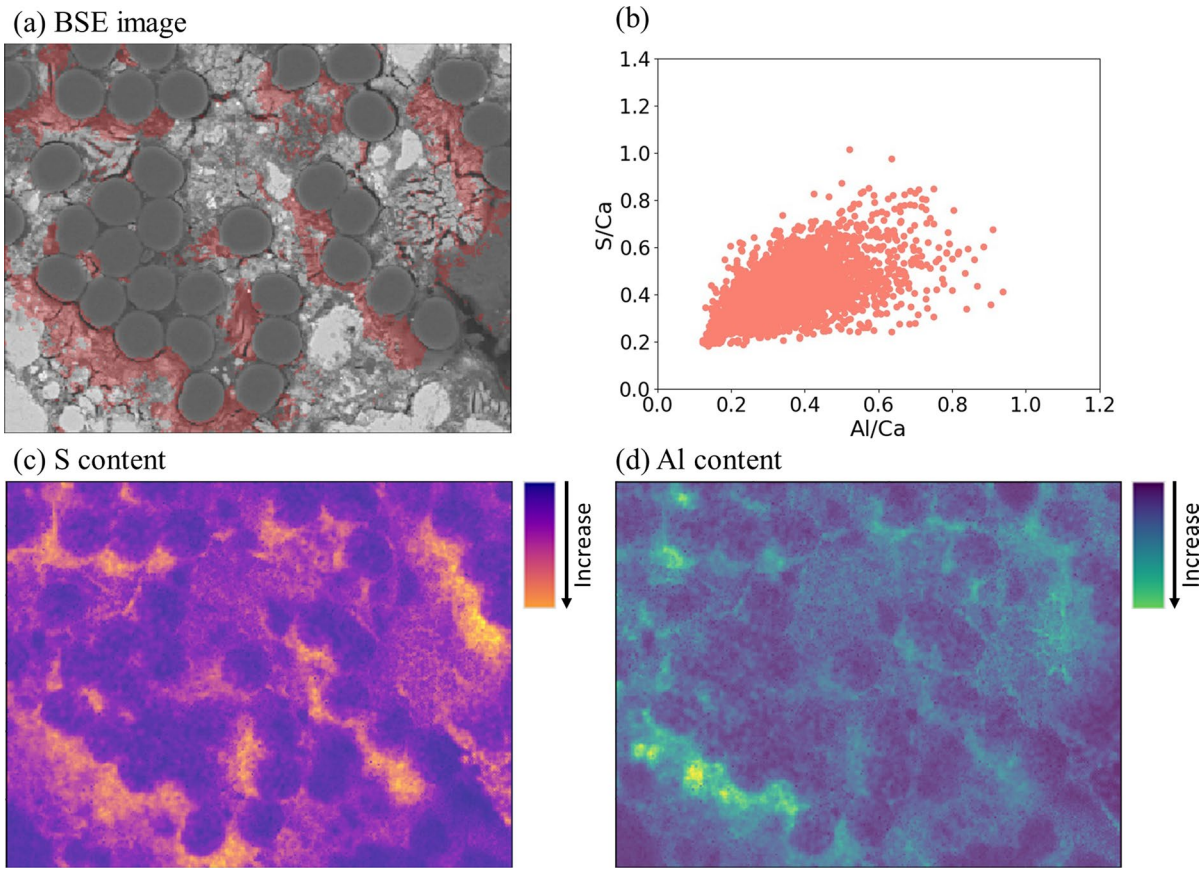

Fig. 12 The EDS map results of BCSA: **a** BSE image, **b** S/Ca via Al/Ca ratio of red zones shown in image (**a**), **c** S element content, **d** Al element content

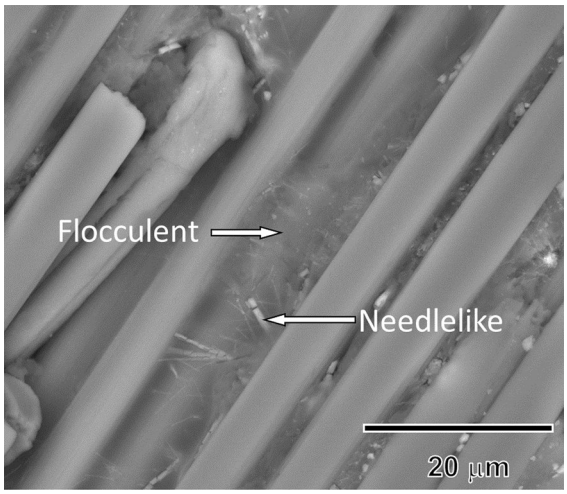

Fig. 13 The SEM image of hydrated products around fibres in BCSA-based composite

along with flocculent hydrated products (probably AH_3). These hydrates grew around the fibres leading to a reduction of the voids, and perhaps, to an increase in the frictional bond between the fibres and the cement paste due to the additional interlock and friction mechanisms at the interface of the two materials. A better compaction of the filaments within the strands has been already seen in the research on glass fibre reinforced cement [44, 45] with OPC matrix modified with calcium sulfoaluminate clinker and metakaolin and such a matrix exhibited an improved frictional bond when compared to the regular OPC binder. Although it is not yet clear whether the needle-like hydrates directly contributed to the mechanical resistance at the interface, it seems that ettringite had its role in improving bond between the binder and the fibres, and helped the fibres to be more efficiently packed. Therefore, the use of the standalone BCSA cement mortars has a clear potential to improve the performance of the existing TRM systems, and hence, boost the recovery of the existing deteriorated RC building stock. However, more research on this topic is due.

5 Discussion

The BCSA mortar showed significantly better bond to the concrete substrate and to the textiles compared to the OPC mortar. The improved bond enhanced the composite action between the materials, which enabled exploiting carbon textiles to a much larger extent, and in consequence, larger stiffness and peak load capacity were attained. In the BCSA series, the largest peak load was developed by BCSA _3C_200_2 and was equal to 22.90 kN, which corresponded to about 200% increase compared to its counterpart with OPC binder. For the OPC series, the largest peak capacity was attained by OPC_3C_150_2 and was equal to 12.19 kN for 150 mm. For the same bond length, the BCSA binder enabled developing a load capacity of 21.55 kN, which corresponds to a 77% increase. The level of utilisation of the fibres was expressed as a ratio between the average experimental axial stress along the warp fibres, σ_{ave}, and the product of $E_f\varepsilon_f$ (equal to 5040 MPa, see Tables 1 and 2), which corresponds to the tensile strength of a single fibre of the carbon textile. It should be noted that such a value of tensile stress can be attained only in an idealised scenario when all fibres of the textile resisting tension are equally mobilised to their maximum tensile capacity. This is usually not achievable in the TRM composites as the mortar paste does not fully penetrate through the fibre rovings, and in turn, the inner fibres have a limited impregnation and do not fully participate in resisting tension. As such, failures related to the textiles often exhibit rupture, but some slippage of the inner fibres is also possible, and this was also evident herein in the case of the BCSA samples. In addition, past experiments documented that the axial stress does not increase proportionally to the number of textile layers and the exploitation of the fibres decrease with the number of layers applied [17], which seemed to have a direct influence in the strengthening efficiency [46]. The OPC results revealed that for the three TRM layers, the maximum stress level was developed for the 150 mm bond length and was just slightly above 800 MPa, which corresponds to about 16% of the fibres' theoretical potential. On the other hand, in the BCSA binder, such exploitation level was already seen for the 50 mm bond length after 35 days of curing, with about 8% utilisation being achieved already after 24 h (for BCSA twin samples with 200 mm bond length tested after 24 h). The maximum level of the tensile stresses in BCSA series was recorded when the failure was in the textile and was equal to 1545 MPa, representing roughly 30% of the tensile strength of a single dry fibre.

Even though such utilisation percentage seems limited for a failure related to the textiles, past experimental studies have demonstrated that loses due to the uneven stress distribution are inevitable. A recent study investigating tensile properties of one TRM layer employing identical textiles embedded in cement-based mortar reported average stress equal to 1174 MPa (about 23% of $E_f\varepsilon_f$) [47]. Tensile tests by D'Antino and Papanicolaou [48] on similar carbon textile grids with 170 g/cm^2 fibres in orthogonal distribution but having a roving grid of 20×20 mm revealed averaged stress of 938 MPa and 1890 MPa for non-coated and epoxy-coated grids, respectively. Finally, for TRMs with similar carbon textile grids a stress value of 986 MPa was reported by Donnini et al. [49] and from 1189 to 2587 MPa by de Santis et al. [50] depending on the test arrangements, with both studies reporting fibre slippage at failure.

The effect of the bond length on the peak load capacity of the TRM is shown in Fig. 14. Past research demonstrated that the bond behaviour of FRP and TRM strips is characterised by a specific behaviour highly affected by the composites' material properties; after a certain bond length, the axial force in the composite strip (which is equal to the anchorage force) tends to reach an almost constant value which is considered as the maximum anchorage force [51], while especially for TRMs it keeps increasing with low stiffness linear indents after

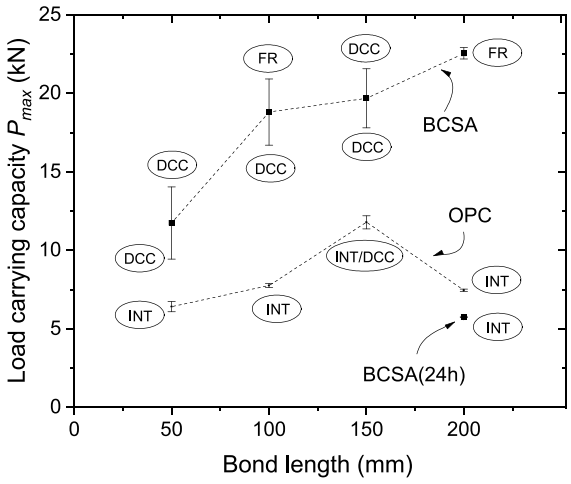

Fig. 14 Effect of bond length on the load bearing capacity (with the corresponding failure modes). The bars represent the range of the results

reaching the effective bond length, [52]. The results of the OPC series showed that the increase in the bond length led to a non-linear increase in the load capacity, which is in agreement with the observations from past experimental studies [17, 19, 20, 22]. The only exception to this was the case of the twin specimens OPC_3C_200_1&2, which exhibited significantly lower load capacity compared to the specimens with the bond length equal to 150 mm. Although the load bearing capacity should not decrease with the increasing bond length, the scatter in such tests can be considerable, especially when different failure modes are present. The drop in the load capacity between the bond lengths 150 mm and 200 mm can be attributed to the slightly different failure modes. OPC_3C_150_1&2 were the only ones from OPC series that showed mixed failure modes involving interlaminar failure (INT) and failure at mortar-concrete interface (DCC). On the other hand, OPC_3C_200_1&2 failed due to interlaminar shearing between the textiles and the mortar on the non-test side (300 mm). The failure on the longer non-test side indicated that effective bond length was already developed also on the test-side, and the failure could occur on either side, whichever has poorer bond. As such, the scatter between these two pairs of samples can be either a product of poor level of the fibre impregnation through the textiles (for OPC_3C_200_1&2) or exceptional bond to the substrate (for OPC_3C_150_1&2). Based on the tests carried out on the OPC series, it can be concluded that effective bond length was somewhere between 100 and 150 mm, and such bond lengths allowed to approach the failure related to the concrete substrate.

The BCSA series showed a clear trend of load capacity increase with increasing bond length until reaching the fibre rupture (FR). The longer the bond length, the larger the load capacity and fibre utilisation. With the increasing bond length, more concrete was engaged in resisting bond stresses and, hence the failure shifted from the concrete to the textile. A larger scatter between two identical tests was observed compared to the OPC series, but this was due to the involvement of two different failure modes at the same bond length, which indicates that between certain bond lengths the concrete substrate was mobilised to a different extent, and the longer the bond length the more textile engagement can be expected. The failure due to the fibre rupture was already seen

for 100 mm bond length (BCSA_3C_100_1), with the other twin sample failing due to DCC at a lower load. A clear result was seen for 200 mm bond length, at which both twin specimens failed due to FR at similar load levels. Hence, despite some mixed failure modes, the anchorage force could already develop at 100 mm bond length, at an even shorter length than for the OPC binder.

It is clear that the BCSA binder, though having similar mechanical tensile properties, showed performance superior to the standard OPC binder in almost every aspect. Figure 6 shows that larger load bearing capacity can be attained, and less anchorage length is required to develop the maximum anchorage force in the strip. In addition, BCSA seems to be able to approach the bond strength and replicate the failure behaviour of the OPC binder already after 24 h of curing (see BCSA(24 h)_3C_50_1&2 in Fig. 6).

The bond of the OPC binder and the fibres seems to be limited due to the gaps at the textile-mortar interface and the hydration products of Portland cement do not exhibit the ability to fill them up as efficiently as BCSA. In turn, the failure in the OPC series actually occurred at this interface and limited potential of this application. As shown through detailed microstructural characterisation, the formation of ettringite around the fibres in the BCSA binder effectively increased the connection between binders and fibres, filling the voids at the interface thereby and resulting in an enhancement of strength. The ettringite phase formed around the fibres turned out to be effective in increasing the chemical bond to the fibres and might be the key to develop stronger binders for TRM applications. It must be also noted that the belite had still not reacted and it is well known that belite forms space/pore filling hydration products and one can infer that this will only further increase the performance; nonetheless this needs to be verified experimentally.

The results presented herein show that the chemistry of the cement has a significant role in the performance of TRM retrofitting system and more research is warranted to better understand the role of the BCSA binder and the ettringite phase in bond to the textile reinforcements. It is suggested that future work should explore more types of textiles but also binders including (sulfo)aluminate cements and ordinary Portland cements with supplementary cementing materials (SCM) in order to develop new generations of sustainable and effective matrices for textile reinforcement.

6 Conclusions

The results presented in this paper provide important insights on the potential of BCSA mortar as a binder for carbon textiles in TRM strengthening applications. The bond of the BCSA TRM to the concrete was determined through modified beam tests on twin specimens investigating different bond lengths and was then compared with counterpart specimens having a standard OPC-based TRM strengthening system applied. Complimentary XRD, TGA, SEM and EDS analyses were also carried out to investigate the chemical bond between the textiles and the mortar, and thus explain better the bond behaviour. Based on the test results and discussion the following conclusions can be drawn:

- Although having similar flexural strength, the BCSA-based TRM system showed performance superior to the OPC-based TRM system. Almost a twofold increase in the load bearing capacity was achieved compared to the OPC series.
- The rapid setting properties of BCSA enabled developing 1-day bond properties close to those of 35-day cured OPC binder.
- BCSA binder enable to exploit textiles' potential to a larger extent utilising the fibres to more than 30% of their nominal mechanical strength.
- The use of BCSA led to a change in the failure modes and shifted the failure from the textile-mortar interface to the textile itself. This was due to the greater bond to the carbon textile and detailed microstructural analysis indicated that ettringite, which developed around the fibres, improved the fibre impregnation.
- The bond length had influence on the failure modes, and thus the utilisation of the textiles. The stronger the binder the stronger the influence of the bond length on failure modes.
- Microstructural characterisation such as XRD, TGA, and SEM was found useful in identifying the chemistry/mineralogy at the binder-matrix interface as well as to visualise the binder-matrix interaction.

Acknowledgements The authors would like to thank CTS Cement Manufacturing Corporation for supplying the BCSA cement, and Paul Russel from MAPEI for providing carbon textiles.

Funding This study was carried out as a part of H2020 Marie Skłodowska–Curie funded research project "THORAX—The next generation of advanced composite materials for sustainable retrofitting of structures" (EU grant agreement 892406). Zhili Ren is funded by INNOVANDI—The Global Cement and Concrete Research Network, a GCCA initiative. Ioanna Skyrianou is funded by the Special Account of Research Grants of University of Thessaly in the operating framework of the Center of Research Innovation and Excellence. Theodore Hanein is funded by UKRI through Future Leaders Fellowship (MR/V023829/1).

Declarations

Conflict of interest The authors declare they have no financial interests.

References

1. American Society of Civil Engineers (ASCE) (2021) 2021 Report Card for America's Infrastructure. https://infrastructurereportcard.org/wp-content/uploads/2020/12/National_IRC_2021-report.pdf. Accessed 1 December 2023
2. European Construction Industry Federation (FIEC) (2021) FIEC 2021 Statistical Report. https://fiec-statistical-report.eu/2021. Accessed 1 December 2023
3. Bakis CE, Bank LC, Brown VL, Cosenza E, Davalos JF, Lesko JJ, Machida A, Rizkalla SH, Triantafillou TC (2002) Fiber-reinforced polymer composites for construction—state-of-the-art review. J Compos Constr 6:73–87. https://doi.org/10.1061/(ASCE)1090-0268(2002)6:2(73)
4. Triantafillou TC (1998) Shear Strengthening of Reinforced Concrete Beams Using Epoxy-Bonded FRP Composites. ACI Struct J 95:107–115. https://doi.org/10.14359/531
5. Barros JAO, Fortes AS (2005) Flexural strengthening of concrete beams with CFRP laminates bonded into slits. Cem Concr Compos 27:471–480. https://doi.org/10.1016/j.cemconcomp.2004.07.004
6. Kotynia R, Cholostiakow S (2015) New proposal for flexural strengthening of reinforced concrete beams using CFRP T-shaped profiles. Polymers 7:2461–2477. https://doi.org/10.3390/polym7111524
7. Rezazadeh M, Cholostiakow S, Kotynia R, Barros J (2016) Exploring new NSM reinforcements for the flexural strengthening of RC beams: experimental and numerical research. Compos Struct 141:132–145. https://doi.org/10.1016/j.compstruct.2016.01.033
8. Koutas LN, Tetta Z, Bournas DA, Triantafillou TC (2019) Strengthening of concrete structures with textile reinforced mortars: state-of-the-art review. J Compos Constr 23:03118001. https://doi.org/10.1061/(ASCE)CC.1943-5614.0000882
9. Triantafillou TC, Papanicolaou CG (2007) Shear strengthening of reinforced concrete members with textile reinforced mortar (TRM) jackets. Mater Struct 39:93–103. https://doi.org/10.1007/s11527-005-9034-3
10. Brückner A, Ortlepp R, Curbach M (2006) Textile reinforced concrete for strengthening in bending and shear. Mater Struct 39:741–748. https://doi.org/10.1617/s11527-005-9027-2
11. Bournas DA, Lontou PV, Papanicolaou CG, Triantafillou TC (2007) Textile-reinforced mortar versus fiber-reinforced polymer confinement in reinforced concrete columns. ACI Struct J. https://doi.org/10.14359/18956
12. Tetta ZC, Koutas LN, Bournas DA (2015) Textile-reinforced mortar (TRM) versus fiber-reinforced polymers (FRP) in shear strengthening of concrete beams. Compos Part B Eng 77:338–348. https://doi.org/10.1016/j.compositesb.2015.03.055
13. Raoof SM, Koutas LN, Bournas DA (2017) Textile-reinforced mortar (TRM) versus fibre-reinforced polymers (FRP) in flexural strengthening of RC beams. Constr Build Mater 151:279–291. https://doi.org/10.1016/j.conbuildmat.2017.05.023
14. Gonzalez-Libreros JH, Sneed LH, D'Antino T, Pellegrino C (2017) Behavior of RC beams strengthened in shear with FRP and FRCM composites. Eng Struct 150:830–842. https://doi.org/10.1016/j.engstruct.2017.07.084
15. Triantafillou TC (2016) Textile fibre composites in civil engineering. Woodhead Publishing, Cambridge. https://doi.org/10.1016/C2014-0-01415-3
16. Kouris LAS, Triantafillou TC (2018) State-of-the-art on strengthening of masonry structures with textile reinforced mortar (TRM). Constr Build Mater 188:1221–1233. https://doi.org/10.1016/j.conbuildmat.2018.08.039
17. Raoof SM, Koutas LN, Bournas DA (2016) Bond between textile-reinforced mortar (TRM) and concrete substrates: experimental investigation. Compos Part B Eng 98:350–361. https://doi.org/10.1016/j.compositesb.2016.05.041
18. D'Ambrisi A, Feo L, Focacci F (2013) Experimental analysis on bond between PBO-FRCM strengthening materials and concrete. Compos Part B Eng 44:524–532. https://doi.org/10.1016/j.compositesb.2012.03.011
19. D'Antino T, Carloni C, Sneed LH, Pellegrino C (2014) Matrix–fiber bond behavior in PBO FRCM composites: a fracture mechanics approach. Eng Fract Mech

117:94–111. https://doi.org/10.1016/j.engfracmech.2014.01.011
20. Sneed LH, D'Antino T, Carloni C (2014) Investigation of bond behavior of polyparaphenylene benzobisoxazole fiber-reinforced cementitious matrix-concrete interface. ACI Mater J. https://doi.org/10.14359/51686604
21. Carozzi FG, Bellini A, D'Antino T, De Felice G, Focacci F, Hojdys Ł, Laghi L, Lanoye E, Micelli F, Panizza M, Poggi C (2017) Experimental investigation of tensile and bond properties of Carbon-FRCM composites for strengthening masonry elements. Compos Part B Eng 128:100–119. https://doi.org/10.1016/j.compositesb.2017.06.018
22. Tran CTM, Stitmannaithum B, Ueda T (2014) Investigation of the bond behaviour between PBO-FRCM strengthening material and concrete. J Adv Concr Technol 12:545–557. https://doi.org/10.3151/jact.12.545
23. Awani O, Refai AE, El-Maaddawy T (2015) Bond characteristics of carbon fabric-reinforced cementitious matrix in double shear tests. Constr Build Mater 101:39–49. https://doi.org/10.1016/j.conbuildmat.2015.10.017
24. D'Antino T, Sneed LH, Carloni C, Pellegrino C (2015) Influence of the substrate characteristics on the bond behavior of PBO FRCM-concrete joints. Constr Build Mater 101:838–850. https://doi.org/10.1016/j.conbuildmat.2015.10.045
25. Carloni C, D'Antino T, Sneed LH, Pellegrino C (2015) Role of the matrix layers in the stress-transfer mechanism of FRCM composites bonded to a concrete substrate. J Eng Mech 141:04014165. https://doi.org/10.1061/(ASCE)EM.1943-7889.0000883
26. Ombres L (2015) Analysis of the bond between fabric reinforced cementitious mortar (FRCM) strengthening systems and concrete. Compos Part B Eng 69:418–426. https://doi.org/10.1016/j.compositesb.2014.10.027
27. Koutas LN, Papakonstantinou CG (2021) Flexural strengthening of RC beams with textile-reinforced mortar composites focusing on the influence of the mortar type. Eng Struct 246:113060. https://doi.org/10.1016/j.engstruct.2021.113060
28. Cholostiakow S, Koutas LN, Papakonstantinou CG (2023) Geopolymer versus cement-based textile-reinforced mortar: diagonal compression tests on masonry walls representative of infills in RC frames. Constr Build Mater 373:130836. https://doi.org/10.1016/j.conbuildmat.2023.130836
29. Cholostiakow S, Skyrianou I, Koutas L, Papakonstantinou C (2023) Out-of-plane performance of structurally and energy retrofitted masonry walls: geopolymer versus cement-based textile-reinforced mortar combined with thermal insulation. Open Res Eur 3:186. https://doi.org/10.12688/openreseurope.16724.1
30. Andrew RM (2018) Global CO_2 emissions from cement production. Earth Syst Sci Data 10:195–217. https://doi.org/10.5194/essd-10-195-2018
31. Hanein T, De La Torre AG, Zhang Z, Provis JL (2022) Alternative non-portland binders. Elements 18:314–320. https://doi.org/10.2138/gselements.18.5.314
32. Hanein T, Galvez-Martos J-L, Bannerman MN (2018) Carbon footprint of calcium sulfoaluminate clinker production. J Clean Prod 172:2278–2287. https://doi.org/10.1016/j.jclepro.2017.11.183
33. Bescher E, Kim J (2019) Belitic Calcium Sulfoaluminate Cement: History, Chemistry, Performance, and Use in the United States. In: Proceedings of the 1st International Conference on Innovation in Low-Carbon Cement & Concrete Technology. London, United Kingdom, pp 23–26
34. Deo O, Bhuskute N, Bescher E, Vaddey NP, Pacheco J (2023) Belitic calcium sulfoaluminate concrete runway. Concr Int 45:27–31
35. Deo O, Win D, Bhuskute N, Chung D, deOcampo N, Bescher E (2022) Fast setting, low carbon infrastructure rehabilitation using belitic calcium sulfoaluminate (BCSA) concrete. MATEC Web Conf 361:00002. https://doi.org/10.1051/matecconf/202236100002
36. Alecci V, Focacci F, Rovero L, Stipo G, De Stefano M (2016) Extrados strengthening of brick masonry arches with PBO–FRCM composites: experimental and analytical investigations. Compos Struct 149:184–196. https://doi.org/10.1016/j.compstruct.2016.04.030
37. Georget F, Wilson W, Scrivener KL (2021) edxia: microstructure characterisation from quantified SEM-EDS hypermaps. Cem Concr Res 141:106327. https://doi.org/10.1016/j.cemconres.2020.106327
38. CEN (1999) Methods of test for mortar for masonry—Part 3: Determination of consistence of fresh mortar (by flow table). European Committee for Standardization, Brussels
39. CEN (2019) Methods of test for mortar for masonry—Part 11: Determination of flexural and compressive strength of hardened mortar. European Committee for Standardization, Brussels
40. Calabrese AS, D'Antino T, Colombi P, Poggi C (2020) Study of the influence of interface normal stresses on the bond behavior of FRCM composites using direct shear and modified beam tests. Constr Build Mater 262:120029. https://doi.org/10.1016/j.conbuildmat.2020.120029
41. Falope FO, Lanzoni L, Tarantino AM (2018) Modified hinged beam test on steel fabric reinforced cementitious matrix (SFRCM). Compos Part B Eng 146:232–243. https://doi.org/10.1016/j.compositesb.2018.03.019
42. Li X, Liu S, Zhang H, Li H, Guan X (2023) Effects of AH_3 and AFt on the hydration-hardening properties of the $C_4A_3S^{-}$-CS^{-}-H_2O system. Materials 16:6322. https://doi.org/10.3390/ma16186322
43. Bizzozero J, Gosselin C, Scrivener KL (2014) Expansion mechanisms in calcium aluminate and sulfoaluminate systems with calcium sulfate. Cem Concr Res 56:190–202. https://doi.org/10.1016/j.cemconres.2013.11.011
44. Purnell P, Buchanan AJ, Short NR, Page CL, Majumdar AJ (2000) Determination of bond strength in glass fibre reinforced cement using petrography and image analysis. J Mater Sci 35:4653–4659. https://doi.org/10.1023/A:1004882419034
45. Purnell P, Short NR, Page CL, Majumdar AJ, Walton PL (1999) Accelerated ageing characteristics of glass-fibre reinforced cement made with new cementitious matrices. Compo Part A Appl Sci Manuf 30:1073–1080. https://doi.org/10.1016/S1359-835X(99)00019-6
46. Koutas LN, Cholostiakow S, Bournas DA, Raoof S, Tetta Z (2024) Optimized hybrid carbon-glass textile-reinforced mortar for flexural and shear strengthening of RC

members. J Compos Constr 28:04023068. https://doi.org/10.1061/JCCOF2.CCENG-4333
47. Estevan L, Varona FB, Baeza FJ, Torres B, Bru D (2022) Textile Reinforced Mortars (TRM) tensile behavior after high temperature exposure. Constr Build Mater 328:127116. https://doi.org/10.1016/j.conbuildmat.2022.127116
48. D'Antino T, Papanicolaou C (2017) Mechanical characterization of textile reinforced inorganic-matrix composites. Compos Part B Eng 127:78–91. https://doi.org/10.1016/j.compositesb.2017.02.034
49. Donnini J, De Caso Y, Basalo F, Corinaldesi V, Lancioni G, Nanni A (2017) Fabric-reinforced cementitious matrix behavior at high-temperature: experimental and numerical results. Compos Part B Eng 108:108–121. https://doi.org/10.1016/j.compositesb.2016.10.004
50. De Santis S, Hadad HA, De Caso Y, Basalo F, De Felice G, Nanni A (2018) Acceptance criteria for tensile characterization of fabric-reinforced cementitious matrix systems for concrete and masonry repair. J Compos Constr 22:04018048. https://doi.org/10.1061/(ASCE)CC.1943-5614.0000886
51. International Federation for Structural Concrete (fib) (2013) fib model code for concrete structures 2010, 1st edn. Ernst & Sohn, Berlin. https://doi.org/10.1002/9783433604090
52. Carozzi FG, Arboleda D, Poggi C, Nanni A (2020) Direct shear bond tests of fabric-reinforced cementitious matrix materials. J Compos Constr 24:04019061. https://doi.org/10.1061/(ASCE)CC.1943-5614.0000991